IEEE Access
Multidisciplinary | Rapid Review | Open Access Journal

Received November 14, 2018, accepted December 14, 2018, date of publication December 21, 2018,
date of current version January 11, 2019.

Digital Object Identifier 10.1109/ACCESS.2018.2889138

Laparoscopic Image-Guided System Based on Multispectral Imaging for the Ureter Detection

FENG YU[1], ENMIN SONG[1], (Senior Member, IEEE), HONG LIU[1], JUN ZHU[1], AND CHIH-CHENG HUNG[2]

[1]School of Computer Science and Technology, Huazhong University of Science and Technology, Wuhan 430074, China
[2]Laboratory for Machine Vision and Security Research, Kennesaw State University, Kennesaw, GA 30144, USA

Corresponding author: Hong Liu (hl.cbib@gmail.com)

This work was supported in part by the National Key Research and Development Program of China under Grant 2017YFC0112804, in part by the Fundamental Research Funds for the Central Universities under Grant HUST: 2017JYCX038 and Grant HUST: 2016YXZD018, and in part by the National Natural Science Foundation of China under Grant 61370179.

ABSTRACT The iatrogenic ureter injury is a common medical negligence in the gynecology, abdominal, and urinary surgeries. Anatomically, the ureter is covered by peritoneum and connective tissue, and the doctor cannot observe it directly in surgery. The ureter injury may cause significant complications for patients and medical disputes. It is important to indicate the ureter position for aided surgery of the doctor. To provide ureter position for doctors in the laparoscopic surgery, we design an image-guided endoscope system that includes a novel endoscopic video system with a visible-light camera and an infrared camera. The visible-light camera is to capture the coeliac image and the infrared camera is to capture the ureter position, simultaneously. To extract accurate ureter position in the infrared image, we also propose a self-adaptive threshold segmentation algorithm to extract the real ureter position as accurately as possible. The self-adaptive threshold and scattering factor are taken in to full account for the ureter segmentation. In addition, the scattering property of light is also discussed to choose the optimal light. Finally, we design and develop the image-guided endoscope system, and experiment it on the animal. The experimental results demonstrate that the proposed image-guided endoscope system achieves 93.8% and 90.6% in terms of true positive rate and positive predictive value, respectively. The processing speed of the proposed algorithm can reach about 165 frames per second (f/s), and the frame rate is far faster than the frame rate (30 f/s) of the traditional endoscope system. The accuracy and processing ability of the system can satisfy the clinical demand. The iatrogenic ureter injury may be decreased when the surgeons perform the operations with the ureter position displayed in real time.

INDEX TERMS Endoscope system, ureter injury, image-guided, multispectral imaging, ureter detection.

I. INTRODUCTION

Iatrogenic ureter injury occurs occasionally in the gynecology, abdominal, and urinary surgeries [1]–[3]. This medical negligence will bring serious effects to both doctors and patients. Under normal circumstance, the ureter is covered by the human tissues [4]–[6], and the doctor cannot observe the ureter during the operation. In surgery, the rich experienced doctors distinguish the ureter by the anatomic relationship. However, the ureter injury also occurs with the different reasons. The doctor may ignore the anatomic relationship between the ureter and other tissues such as the uterine artery, colic artery, spermatic vein, and inferior mesenteric artery. The tissues are covered by the peritoneum, and the shapes are very similar. To dissociate the ureter, the doctor should dissociate other similar tissues one by one. The tissue adhesion and excessive bleeding also increase the difficulty to distinguish the ureter. The normal anatomical position of ureter may change when the condition of tumor adhesion and extrusion occurs. In this complex circumstance, the ureter injury takes place easily even for very experienced doctors [7], [8]. The ureter injury may cause serious complications for the patient, such as urinary extravasation, urinary fistula, hematuria, lumboabdominal pain, and fever. Furthermore, the ureter injury is usually found after the operation. Without the timely treatment, the serious complications may be life-threatening for the operating patient. Hence, with the endoscope widely used [9]–[12], the medical negligence of ureter injury is increased [7], [13].

Therefore, it is necessary to recognize the ureter position for the doctor in surgery. This issue attracts many attentions nowadays but without an effective method to indicate ureter position in clinic. Some doctors insert the double J-tube [14] or ureteral catheter [15], [16] into the ureter to mark the ureter. In order to recognize the real ureter position, the doctor should touch the suspected pipes in the abdominal cavity. If the doctor find that the suspected pipe is hard, and the pipe may be the ureter. However, the doctor's hands cannot reach the ureter in the minimally invasive surgery, and the method only can be used in the open surgery. The doctor uses the operating forceps to process the surgery in the minimally invasive surgery, and it is difficult to perceive the hardness of the suspected pipes. Furthermore, the method cannot provide the real-time visible sense for the doctor. Some doctors use a light pipe to mark the ureter in the clinical trials [17], but the light pipe is difficult to be captured by the endoscope system under the strong endoscopic light. And the method is not applied in clinic so far. The ultrasound-guided [18] technology is also used to indicate the ureter position, but it cannot provide the whole visual image of the ureter for the doctor. Except for above methods, some doctors use the intravenous pyelography and retrograde pyelography to recognize the ureter, but these methods are used in pre-operation. The near-infrared fluorescence (*NIRF*) technology [19]–[22] is proposed to recognize the ureter in recent years. However, the fluorescence is too weak to penetrate the ureteral wall, and the ureter can be detected when the ureter is partially exposed. In [23], a novel endoscope system which can display the ureter position is proposed. It is the first endoscope system that can automatically detect the ureter position, but the displayed images exist slightly flickering phenomenon. To remove the flickering phenomenon, [24] proposes the ARES-UPD with the encoded endoscopic light to detect the ureter position. In [25], the IGES-UD based on the infrared is proposed to detect the ureter position. The detective ability and processing speed are better than previous works [23], [24].

In this system, in order to further improve the detective ability and processing efficiency, we propose an image-guided endoscope system based on the multispectral imaging for the ureter detection. Under normal circumstance, the ureter cannot be detected by the endoscopic camera. We use the infrared imaging technology to realize the ureter detection. A pipe with infrared light is used to mark the ureter position, and two cameras that includes a visible-light camera and an infrared camera are used to capture the coeliac image and the ureter position. This method significantly improves the detective ability of the ureter. In addition, we design and develop a novel endoscope system which includes the hardware and software systems to evaluate the performance of the proposed system. The animal experimental results demonstrate that the image-guided endoscope system can obtain the accurate ureter position in real-time. The imaging quality and processing speed are also better than our previous systems [23]–[25].

Compared with the traditional endoscope system, the image-guided endoscope system realizes the function of the ureter detection in real-time. We modify the system structure of the traditional endoscope system, and propose a novel imaging method for the ureter detection. The system not only has the function of the traditional endoscope system, but also the function of the ureter display. The innovations are shown as following.

1) Technology innovation: The proposed image-guided endoscope system resolves the problem of the ureter display, and will reduce the medical negligence that the ureter is easy to be damaged during the surgery. In the laparoscopic surgeries, the doctor should recognize the ureter that cannot be captured by the traditional endoscope system for avoiding damaging the ureter. The proposed system can display the ureter position in real-time for realizing the function of assisted surgery.
2) System structure innovation: The novel system structure based on the multispectral imaging is proposed to solve the problem that the ureter is difficult to be detected. The novel endoscope video system based on the infrared for the ureter detection is first designed in the endoscope system. The camera can easily capture the infrared signal of the pipe inserted in the ureter. Furthermore, because the visible-light imaging system is not disturbed by the infrared light, the final displayed images will have high-quality imaging.
3) Theory innovation: To accurately segment the ureter position, we propose the *SATS* algorithm. The segmented threshold can be automatically obtained, and the scattering factor is used to obtain the optimal threshold to reduce the over-segmentation. Experimental results illustrate that the algorithm can achieve the accurate ureter position in real-time.

The remainder of this paper is organized as follows: Section 2 introduces the system architecture and the ureter imaging methods that include image acquirement, ureter extraction, and image fusion. Section 3 gives the system implementation and the system evaluation. Section 4 discusses the importance of the proposed image-guided endoscope system and its future directions. The Section 5 concludes the paper.

II. SYSTEM ARCHITECTURE AND IMAGING METHODS

There are two key issues for the ureter detection. One is how to mark the ureter position. Under normal circumstance, the ureter is covered by the human tissues, and the traditional endoscope system cannot capture the ureter information. We should use some method to mark the ureter, and make it generate some signal. Another issue is how to detect the signal from the ureter under the strong endoscopic light. In this section, to solve the issues, we design a novel endoscopic system architecture, and propose new imaging methods for the ureter detection.

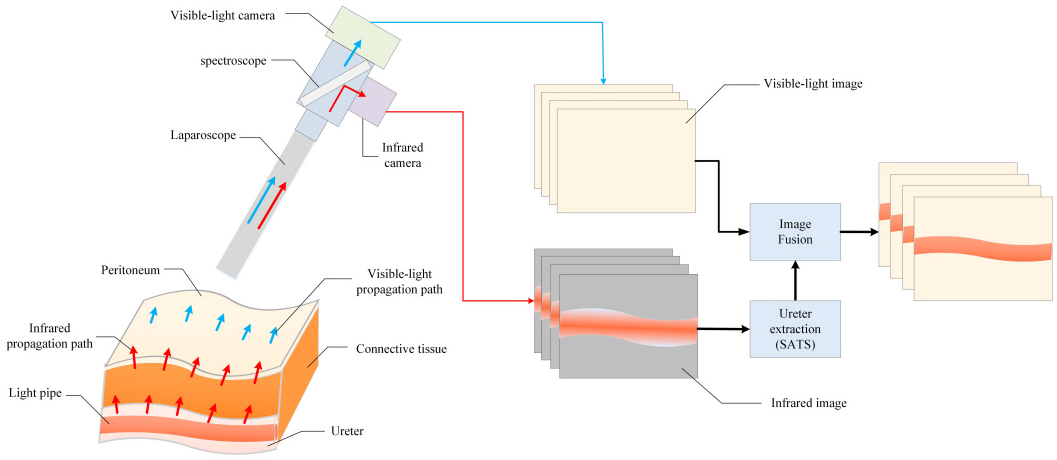

FIGURE 1. The system architecture of the image-guided endoscope system.

A. SYSTEM ARCHITECTURE

To realize the function of the ureter detection, we design the image-guided endoscope system. The system architecture is shown in Figure 1 that gives the schematic diagram of the proposed system. Before executing the surgery, a pipe is inserted into the ureter. The pipe is similar to the ureteral catheter in terms of the shape. The pipe is linked with an infrared light, and the whole pipe will give out light. The insertion operation is same as usual insertion operation of the ureteral catheter. The endoscopic images are captured by the designed endoscope video that includes two cameras with different imaging spectrums. Because the infrared camera only captures the infrared light [26], [27], we use the infrared camera to capture the pipe inserted in the ureter. Furthermore, we propose the *SATS* algorithm to achieve the precise ureter position. The coeliac image is captured by the visible-light camera. These two images are used to generate the output image displayed in the endoscopic monitor.

B. IMAGE ACQUIREMENT METHOD

There are two key issues for acquiring the ureter information. One is the choice of the medium which should have good characteristics of light transmission. Because the ureter is covered by the human tissues, the indicated light should penetrate the light-guided medium as much as possible. The non-toxic of light-guided medium is also necessary requirement in our experiments. Thus we choose a surface-lighting plastic optical fiber (*POF*) [28], [29] as the light-guided medium. The light will penetrate from the inner of *POF* to outside. The input light is not only reflected but also refracted in the *POF*. Thus, we can observe the light on the whole *POF*. The outer layer of *POF* can choose the medical polymer material, such as Poly Methyl Methacrylatemethacrylic Acid (*PMMA*) [30], [31], Poly Tetra Fluoro Ethylene (*PTFE*) [32], [33], and others. The *POF* mainly includes two components: outer layer and central layer, and the schematic diagram is shown in Figure 2.

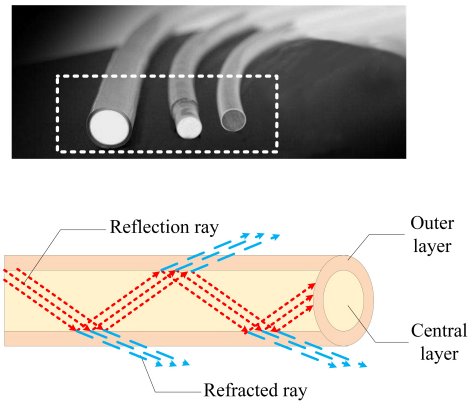

FIGURE 2. The structure of POF.

Another key issue is the choice of the light. The different wavelength lights have different attenuation properties. In order to choose the optimal light which can penetrate the human tissues as much as possible, we investigate five different common lights to analyze their characters of attenuation. The LED cold light (80 W), green laser (80 mW of power, 525 nm of wavelength), red laser (250 mW of power, 655 nm of wavelength), 940 nm infrared light (10 W of power), and 850 nm infrared light (10 W of power) are chosen for testing. The pipe is covered with the chicken intestine and about 2 mm thickness of adipose tissue. The ureter images are captured under the opened and closed endoscopic light respectively. The average grayscales of captured ureter images are shown in Figure 3.

From Figure 3, without the endoscopic light, the average grayscale of ureter region is large enough for the ureter detection. While the endoscopic light is on, the ureter position is covered by the strong endoscopic light, and the weak light from the pipe is difficult to be detected. The experiments indicate that the infrared light (850 nm) still can be captured enough brightness for the ureter indication under the strong endoscopic light. Thus, we choose the infrared light (850 nm)

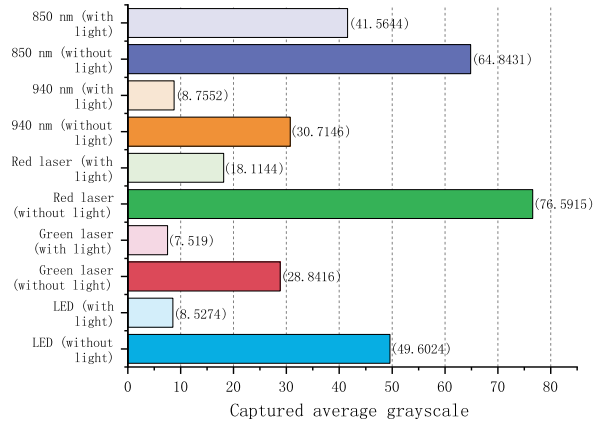

FIGURE 3. The transmission performance of different lights.

TABLE 1. The decrement of different lights.

Light	LED	Green laser	Red laser	940 nm infrared	850 nm infrared
Decrement (%)	82.81	73.93	76.35	71.50	35.90

as the light source for the pipe in our system. These phenomena demonstrate that the visible light is easily covered by the strong endoscopic light, and the grayscale difference between opening and closing light is conspicuous. From Table 1, except for the 850 nm infrared light, other lights are decreased from about 70% to 80%.

C. URETER EXTRACTION ALGORITHM

Actually, the ureter region of infrared image is larger than the real ureter. This phenomenon is caused by the scattering of the light. To extract precise ureter position from the infrared image, we propose the *SATS* algorithm which automatically chooses the initial threshold and adds a scattering factor. The fundamental idea of *SATS* is from the *OTSU* method [34], [35], but the *OTSU* method cannot solve the scattering issue. The *OTSU* method is used to obtain the initial threshold for the *SATS* algorithm. Then, the scattering factor is used to obtain the precise ureter position.

The initial threshold $T_{initial}$ is obtained by Equation (1).

$$max\ [\sum_{i=0}^{c-1}\frac{n_i}{n}(URETER-\sum_{i=0}^{g-1}i\frac{n_i}{n})^2 + \sum_{i=c}^{g-1}\frac{n_i}{n}(BACKGROUND-\sum_{i=0}^{g-1}i\frac{n_i}{n})^2] \tag{1}$$

$$URETER = (\sum_{i=0}^{c-1}i\frac{n_i}{n})/(\sum_{i=0}^{c-1}\frac{n_i}{n}) \tag{2}$$

$$BACKGROUND = (\sum_{i=c}^{g-1}i\frac{n_i}{n})/(\sum_{i=c}^{g-1}\frac{n_i}{n}) \tag{3}$$

where n_i is the number of pixels with grayscale v_i; n is the total number of pixels in the infrared image, and c is the initial grayscale threshold of the first class. The grayscale of first initial group is $[0, 1, \cdots, c-1]$, and the other group is $[c, c+1, \cdots, g-1]$. *URETER* denotes average grayscale of the ureter position; and *BACKGROUND* is the average grayscale of the background.

Since the light exists the phenomenon of scattering in the human tissues, the segmented region will be larger than the real ureter. Thus, the scattering factor is considered in the optimal threshold to reduce the over-segmentation. According to the scattering characteristic, the scattering factor ξ should be added to the initial threshold.

$$T_{optimal} = T_{initial} + \xi \tag{4}$$

The choice of scattering factor ξ is based on the scattering characteristic of light [36] in human tissues. The detailed discussion of the ξ is given in Section III-B.1. After obtaining the optimal threshold, the ureter position is segmented using Equation (5).

$$P_{ureter} = \begin{cases} 255 & \text{if } P_{gray} \geqslant T \\ 0 & \text{if } P_{gray} < T \end{cases} \tag{5}$$

where P_{gray} is the grayscale of the captured infrared image; P_{ureter} is the grayscale of ureter position. The corresponding position of P_{ureter} in the infrared image is the extracted ureter position.

D. IMAGE FUSION ALGORITHM

The output image of the image-guided endoscope system includes the coeliac image and the ureter position. The visible-light image should be fused with the segmented ureter position. From the visible-light image $V_{i,j}^{R,G,B}$, we can obtain the image of coeliac tissues. The ureter position is extracted by the *SATS* algorithm as described in Section II-C. In order to indicate the ureter position but does not disturb doctors' operations, the semitransparent color is chosen for display. Because the green color is rare in the human abdominal tissues, we choose the green color to mark the segmented ureter position. In addition to this, other differentiated colors also can be chosen as the marking color.

Generally, the visible-light camera almost cannot capture the infrared light, and the visible-light image does not include the ureter position in the actual application. In this system, we choose the green as the marking color, so the channel of G is chosen to be processed as Equation (6).

$$V_{i,j}^{G'} = V_{i,j}^{G} + U_{i,j} \tag{6}$$

$$F_{i,j} = V_{i,j}^{(R,G',B)} \tag{7}$$

where $V_{i,j}^{G'}$ is the visible-light image of the enhanced G channel; the segmented ureter position in the infrared image is described as $U_{i,j}$; i, j is the coordinate of the image; G' is the fused channel of G in the visible-light image. The final output image is denoted by $F_{i,j}$. R, G *and* B are three channels of the visible-light image.

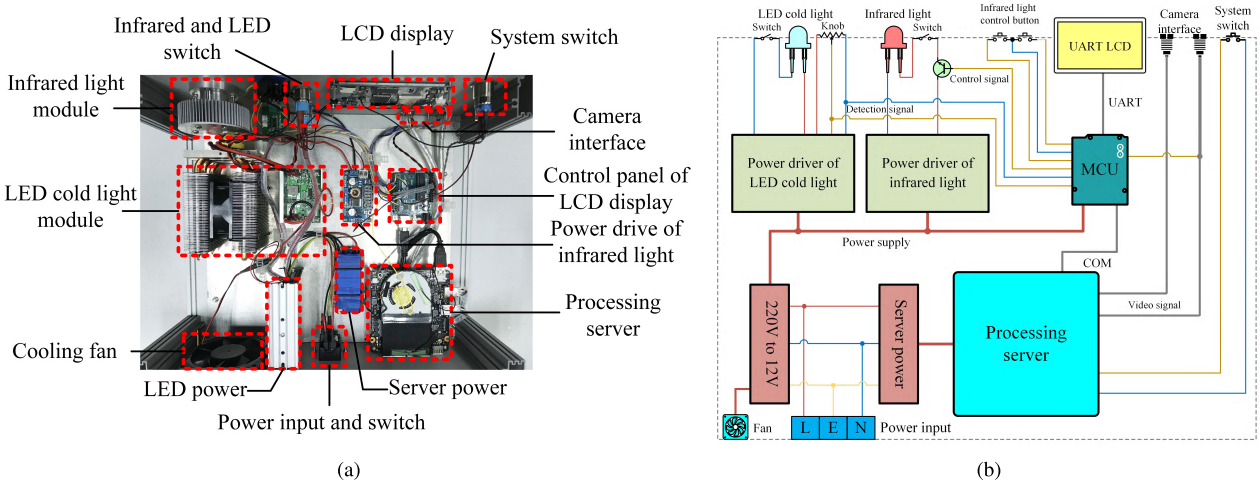

FIGURE 4. The developed endoscope system. (a) The real endoscope system. (b) The electrical schematic diagram.

III. SYSTEM IMPLEMENTATION AND EVALUATION

To evaluate the proposed image-guided endoscope system, we design and implement the endoscope system. The endoscope system mainly includes the endoscope host system and endoscope video system. The endoscope host system mainly provides the function of the image processing, and the endoscope video system is used to capture the coeliac image and the ureter position. Finally, the system is applied and evaluated by the animal experiment.

A. SYSTEM IMPLEMENTATION

The developed system includes hardware and software components. The endoscope host system and video system are the key components in the hardware system. The endoscope host system (Figure 4(a)) mainly includes a processing server, an infrared light module, a LED cold light module, a LED power, a server power, and other auxiliary equipment. The hardware system is used to capture the image, process the captured image, and provide the infrared and LED lights. To further reveal the schematic of the endoscope host system, we also give the electrical schematic diagram in Figure 4(b) that reveals the connected relation of all the components in the host system. In addition, we develop the software system that is easily used to be operated in the clinical experiments for the doctor. The software system is installed in the processing server before running the system.

The developed endoscope video system as shown in Figure 5, and it mainly includes a visible-light camera, an infrared camera, and a spectroscope. The light path from the abdominal cavity is separated into two branches by the spectroscope, and goes into the visible-light and infrared cameras, respectively. The laparoscope is a common endoscope used in the laparoscopic surgery.

B. SYSTEM EVALUATION

The accuracy of the ureter position and the processing speed are the key indicators in the image-guided endoscope system.

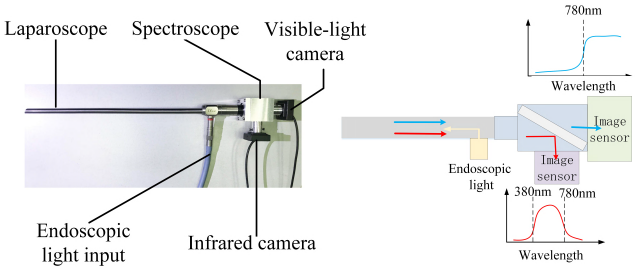

FIGURE 5. The endoscope video system.

The high accuracy of the system can give the accurate ureter position for the doctor. The real-time performance of the system can provide the real-time display of the output images for the operating doctor.

The true positive rate ($TPR = TP/(TP+FN)$), the positive predictive value ($PPV = TP/(TP+FP)$), accuracy ($ACC = (TP+TN)/(TP+TN+FP+FN)$), and the F_1 ($F_1 = 2TP/(2TP+FP+FN)$ are the common indicators for the evaluation of the segmentation performance. The definition of four basic parameters (TP, TN, FP, and FN) can be obtained in [24] and [25]. Actually, it is difficult to obtain the ground truth of the ureter position. In order to mark the real position of ureter as accurate as possible, we dissociate the ureter after experiments, and mark the ureter position based on the real ureter position and visible-light images. Although the marked ureter position is not absolutely precise, the position is still worthy to be evaluated with the segmented ureter position.

The frame rate of the image display is another key indicator. The frame rate of the traditional endoscope system can reach the 30 f/s or up. Thus, the processing speed of the proposed endoscope system should be close to 30 f/s or up. It means that the processing speed of each frame image should be less than 0.033 seconds. In this system, the time cost mainly includes the time of image segmentation and image fusion, and we should reduce the time cost as much as possible in these procedures.

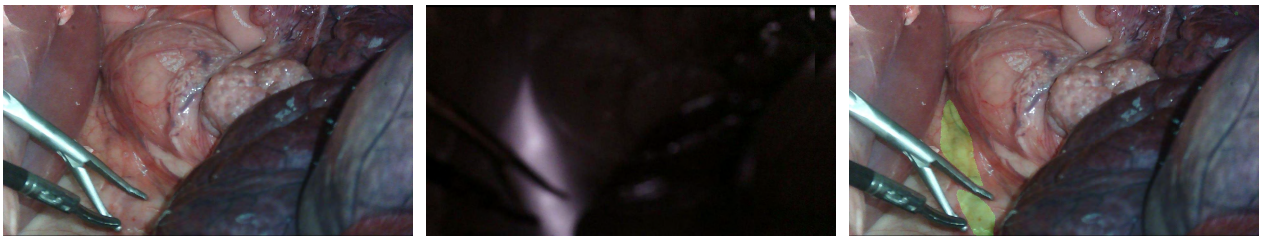

(a) (b) (c)

FIGURE 6. The processing of image fusion. (a) The visible-light image. (b) The infrared image. (c) The fused image.

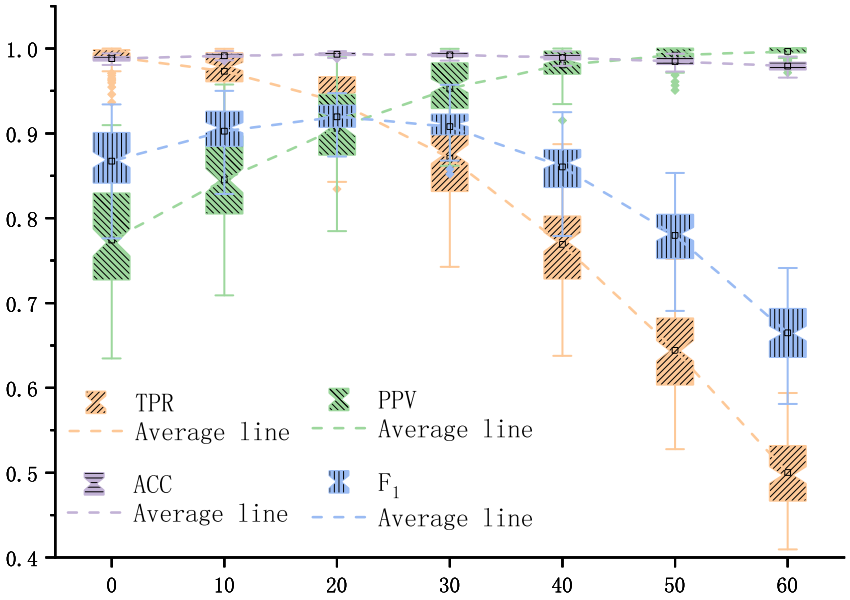

FIGURE 7. The accuracy with different threshold.

In our evaluation experiments, we use the computer with the Matlab 2016 to process and evaluate the accuracy and processing speed. The basic hardware configuration of the computer includes Intel i5-4570 CPU, Nvidia GeForce GTX 750 graphics card, and 16 GB Kingston memory chips.

In this experiment, the used animal is a sow with the weight about 60 kg. Before the simulated surgery, the sow is anesthetized with the propofol. With the surgery processing, the propofol is being injected intravenously. The sow is breathed by the manual resuscitator bay during the surgery. The laparoscope is inserted into the pig's abdominal cavity, and capture the images.

After setting up the experimental platform, the proposed image-guided endoscope system can be used in the animal experiments to evaluate the performance of the system. First, the visible-light and infrared cameras capture the images of abdominal cavity simultaneously. The captured images are shown in Figure 6. From Figure 6(b), we can easily obtain the ureter position, and the accurate position is extracted by the *SATS* algorithm as described in Section II-C. Then, the procedure of image fusion is processed by Equation (6). The processed result of image fusion is shown in Figure 6(c).

1) THE PERFORMANCE EVALUATION

In order to evaluate the performance of the proposed image-guided endoscope system, 100 pairs of images from the 1889 pairs are randomly selected. The TPR, PPV, ACC, and F_1 are used to evaluate the accuracy at different standpoints. From Figure 7, we can know that if the threshold is increased, the TPR will be decreased, the PPV will be increased, and ACC and F_1 will be increased first and then decreased. When the scattering factor ξ is 20, the ACC and F_1 have the maximum, and the TPR and PPV have a point of intersection. The experimental results indicate that the TP and FP are decreased with the increasing threshold, and it causes that the TPR is decreased and PPV is increased. The point of intersection indicates that the segmented result has the maximum coselection rate with the ground truth. Thus, the optimal segmented result is at the intersection.

TABLE 2. The comprehensive comparison of different methods.

Methods	Basic principle	Accuracy	Processing speed (second)	Available time	Available phase
Ureteral stent	Touch	N/A	N/A	All	Intraoperation
Lighted ureteral stent	Visible light detection	N/A	N/A	All	Intraoperation
Ultrasound guided	Ultrasound imaging	N/A	N/A	All	Intraoperation
Near-infrared Fluorescence	Fluorescence imaging	N/A	about 0.07	$10 \sim 60$ minutes	Intraoperation
Intravenous pyelography	CT imaging	N/A	N/A	N/A	Pre-operation
Retrograde pyelography	CT imaging	N/A	N/A	N/A	Pre-operation
ES-PDDE [23]	Visible light enhancement detection	$2 \sim 8$ pixel error	about 0.16	All	Intraoperation
ARES-UPD [24]	Visible light enhancement detection	92.04% TPR	about 0.28	All	Intraoperation
IGES-UD [25]	Infrared light enhancement detection	83.54% TPR	about 0.04	All	Intraoperation
Current system	Infrared light enhancement detection	93.8% TPR	about 0.00607	All	Intraoperation

In addition, the processing time is also the important index for the clinical application. In the clinical endoscope system, the frame rate is about 30 f/s. Thus, the processing time should be less than 0.033 s in our proposed system. According to the experiment, we randomly select 100 pairs of images to count the average processing time. The experimental result indicates that the average processing time is about 0.00607 s.

2) THE COMPARISON WITH OTHER URETER DETECTION METHODS

A comparison of different ureter detection methods are reviewed in Table 2. We discuss the comparison from the five different indicators of the different methods. The basic principle gives the fundamental detection method of the ureter. The detected accuracy of the ureter position is given in the accuracy. The processing speed indicates the processing time of each frame image, and it denotes the frame rate of the different methods. The available time is the service time of the method in surgery. The available phase is the detective phase of the ureter position. Based on the significance of the ureter position, we only discuss the situations of intraoperation and pre-operation. The ureter detection of postoperation is usually as the postoperation review in the urinary surgery. Because some traditional detective methods are manual or non-intelligent, a few detailed information cannot be quantized and verified, and the information is expressed as "N/A." Although some detailed indexes of traditional method cannot be compared, the methods are still worthy to be compared together.

The ureter position is very important during the surgery. The basic operations of the doctor need keep off the ureter at every moment to avoid damaging the ureter. The detective methods of intravenous pyelography and retrograde pyelography are all used before the surgery, and the pre-operative ureter position cannot provide the real-time position for the doctor. The ultrasound-guided method also can achieve the ureter position, but the ureter imaging is transverse section which is not visualized for surgeons. The ureteral stent is the common method that is used for marking ureter, but it cannot provide the visual position information. The doctor recognizes the ureter by touching the suspected intestinal tube, because the ureter inserted a stent is hard. With the popularity of the minimally invasive surgery, the method of the ureteral stent is difficult to be used in the modern surgery. Although the lighted ureteral stent can provide the visual position, its light is easy to be covered by the endoscopic light. The method is merely used in a few trials. The near-infrared fluorescence imaging detects the ureter position by injecting intravenously the dye. With the urine flowing, the dye which is excited by the laser can be detected by the near infrared camera. Although the fluorescence imaging can obtain the ureter position with the dye, the detective ability is too weak to be useful in clinic. However, with the consumption fo the dye, the detective signal of the ureter position will be increasingly weak. In the ES-PDDE [23], the visible-light enhancement detection is used to indicate the ureter position. The advantage of the ES-PDDE compared with other methods is that the system is more automatic and more intelligent. In the ARES-UPD [24], the imaging quality and speed are improved than the ES-PDDE. Reference [25] uses the multispectral camera to detect the ureter marked by the infrared light. The detectability of the ureter is improved, and reduce the complexity of the processing algorithm. In the current system, we design the image-guided endoscope system to obtain the ureter position. The quality of output

image is further improved than the systems of ES-PDDE and ARES-UPD, because the infrared camera has stronger detectability than the visible light under the strong endoscopic light. In [23] and [24], the methods are used to mainly enhance the weak signal of the ureter position under the strong endoscopic light. In this system, we design the multispectral imaging system that includes visible-light and infrared cameras for the image acquirement. Because the infrared camera is specially used for obtaining the ureter position, the ureter signal cannot be disturbed by the endoscopic light, and the detectability of this system is stronger than [23] and [24]. In addition, this system uses the multi-camera imaging system, the two cameras can capture visible-light and infrared, respectively. Thus, compared with [25], the imaging quality is further improved. The ureter position is easily segmented in the infrared image, and the algorithm complexity of the image segmentation is also easier than [25].

IV. DISCUSSION AND FUTURE DIRECTIONS

A novel endoscope system based on the multispectral imaging is proposed to recognize the ureter position. According to the experimental results, the proposed image-guided endoscope system can obtain accurate ureter position with the fast processing speed. Because the infrared camera is used in the system, the captured ability of the weak ureter information is enhanced. By the animal experiments, the accuracy and speed of extracted ureter position are satisfied with the clinical demand.

Generally, there are some tissues cover the ureter, the doctor cannot directly observe the ureter in surgery. In addition, the traditional endoscope system cannot capture the ureter inserted a lighted pipe under the strong endoscopic light. The endoscopic light will cover the weak light from the pipe. Thus, we use the *POF* to mark the ureter position, and design a multispectral endoscope system which includes visible-light and infrared cameras to capture different images. Another advantage of the proposed system is that the marked ureter by infrared light cannot be influenced by the endoscopic light. This advantage may significantly improve the detective ability of the ureter.

Through a limited number of lights which are tested in our experiments, we find that the 850 nm infrared light satisfies our demand. Under the strong LED light, the infrared camera still captures the obvious infrared light from the pipe inserted into the ureter. On the contrary, the LED light, red laser, green laser, and 940 nm infrared light have the inferior performance in terms of penetration. Hence, the choice of indicated light is also significant in our system. Maybe the better light source is satisfied our system, however, the 850 nm infrared light is the best choice in our system in our experiments.

Apart from the systems of ES-PDDE, ARES-UPD, and IGES-UD, the current system is the most possibly used to obtain the intraoperative ureter position in clinic. The proposed image-guided system has significant improvement compared with our previous proposed systems. We design a novel imaging system and imaging method for the ureter detection. In the ES-PDDE system, the final images are fused by the bright and dark images. However, the bright images exist the grayscale difference in the video stream, the final fused images may cause the visual fatigue for the doctor. The display of the ureter is generated by the curve fitting method, and the method has extensive computation complexity which will reduce the processing speed. Hence, the imaging quality and processing speed are not as good as this proposed system. In the ARES-UPD, the endoscopic light adopts stable light source, and the bright and dark frames are captured based on the status of the twinkling *POF*. The ureter position is processed by the monochrome channel filtering algorithm and automatic region growing algorithm. The imaging quality and speed are improved in comparison to the ES-PDDE. The ES-PDDE and ARES-UPD obtain the ureter position with the visible light to mark the ureter. The differences between them are that adopt the different marking styles and propose different image segmentation algorithms. In order to improve captured signal strength from the ureter, the IGES-UD adopts the infrared light to mark the ureter for the first time. The IGES-UD can reduce the effect of the strong endoscopic light, and capture the conspicuous signal from the ureter. The detective ability and processing speed are further improved than previous works [23], [25]. The fluorescence imaging technology was also proposed to indicate the ureter position in the past. Although the method can obtain the intraoperative ureter position, it has some disadvantages that may reduce the convenience and availability in surgery: 1) the fluorescence signal is not strong enough to support the ureter visualization for the surgeon during laparoscopic surgery [22], and the close proximity is required between the endoscope and the ureter to obtain the fluorescence signal, 2) as the urine flow in the ureter is not continuous, and the fluorescence signal is related to the urine flow. Thus, the fluorescence signal will be varied with the change of urine flow during the surgery [21], 3) the frame rate of fluorescence imaging is about 15 f/s in the procedure of merged image [19]. However, the traditional real-time frame rate is 30 f/s in the traditional endoscope system, and 4) the patient should be notified that intravenous dye injection could potentially cause the serious anaphylactic reaction, even though this risk is very low to negligible [22].

The endoscope system with the function of the ureter display can indicate the ureter position during the surgery. The real-time indication of the ureter can help the doctor recognizes the ureter without excessive caution. The function may shorten the operation time and reduce the anesthetic effective time of the operating patient. The more importance is that the system may reduce the medical accident of iatrogenic ureter injury if the image-guided endoscope system is used in clinic.

In addition, with the development of artificial intelligence and cloud computing technologies, the endoscopic image analysis [37], [38] and big healthcare data [39], [40] should further improve the intelligence and automation of the endoscope system. The endoscopic image analysis can realize the aided diagnosis with the advanced image processing algorithms for the doctors. Furthermore, the future system can use

the cloud storage technology to realize the intelligent management of endoscopic date. The artificial intelligence and cloud computing technologies may improve the intelligence of the traditional medical systems in the future.

V. CONCLUSIONS

A novel laparoscopic image-guided system based on the multispectral imaging is proposed for the ureter detection. To realize the function of the ureter detection in surgery, we design the novel endoscope host system and the endoscope video for the laparoscopic image acquirement and processing, and the *POF* with the infrared light is used to mark the ureter. In order to improve the detectability of the ureter, we use the designed multispectral imaging camera to capture the laparoscopic image. Because the captured ureter image exists the phenomenon of light scattering and reflection, the obtained ureter position is not precise enough. And we propose the *SATS* algorithm to segment the ureter to extract accurate ureter position. The segmented ureter position and the visible-light image are fused into the output image. The animal experiments are performed to evaluate the proposed image-guided endoscope system. Experimental results demonstrate that the proposed system obtains 93.8% and 90.6% accuracy in the terms of *TPR* and *PPV*. The system with low computation cost can maintain frame rate of 165 f/s in the clinical application. The processing speed is faster than the frame rate (30 f/s) of the traditional endoscope system, and the performance satisfies the clinical demand. The iatrogenic ureter injury may be reduced when the proposed image-guided endoscope system is used in clinic. In the future work, the human clinical trials should be executed to further evaluate the stability and robustness of the proposed image-guided system.

REFERENCES

[1] V. T. Packiam, A. J. Cohen, J. J. Pariser, and G. T. Bales, "The impact of minimally invasive surgery on major iatrogenic ureteral injury and subsequent ureteral repair during hysterectomy: A national analysis of risk factors and outcomes," *Urology*, vol. 98, pp. 183–188, Dec. 2016.

[2] A. Franklin, N. Pokala, C. Jones, C. Johans, K. Strom, and J. Cummings, "Is the robotic approach feasible for repair of iatrogenic injuries of the lower ureter," *World J. Urol.*, vol. 34, no. 9, pp. 1323–1328, 2016.

[3] T. Karakan *et al.*, "Evaluating ureteral wall injuries with endoscopic grading system and analysis of the predisposing factors," *J. Endourol.*, vol. 30, no. 4, pp. 375–378, 2016.

[4] W. C. de Groat and N. Yoshimura, "Anatomy and physiology of the lower urinary tract," in *Handbook of Clinical Neurology* (Part of volume: Neurology of Sexual and Bladder Disorders), vol. 130, no. 3. Amsterdam, The Netherlands: Elsevier, 2015, ch. 5, pp. 61–108, doi: 10.1016/B978-0-444-63247-0.00005-5.

[5] R. Mulţcescu, D. Georgescu, P. A. Geavlete, and B. Geavlete, "Notions of histology, anatomy, and physiology of the upper urinary tract," in *Retrograde Ureteroscopy: Handbook of Endourology* (Part of volume: Retrograde Ureteroscopy). Amsterdam, The Netherlands: Elsevier, 2016, ch. 2, pp. 7–19, doi: 10.1016/B978-0-12-802403-4.00002-4.

[6] Z. Moinuddin and R. Dhanda, "Anatomy of the kidney and ureter," *Anaesthesia Intensive Care Med.*, vol. 16, no. 6, pp. 247–252, 2015.

[7] P. Andersen, L. M. Andersen, and L. H. Iversen, "Iatrogenic ureteral injury in colorectal cancer surgery: A nationwide study comparing laparoscopic and open approaches," *Surg. Endoscopy*, vol. 29, no. 6, pp. 1406–1412, 2015.

[8] W. S. Orr, L. L. Pisters, and M. A. Rodriguez-Bigas, "Intraoperative ureteral injury," in *Gastrointestinal Surgery*. Springer, 2015, pp. 361–370, doi: 10.1007/978-1-4939-2223-9_34.

[9] O. Gloger, B. Lehnert, A. Schrade, and H. Völzke, "Fully automated glottis segmentation in endoscopic videos using local color and shape features of glottal region," *IEEE Trans. Biomed. Eng.*, vol. 62, no. 3, pp. 795–806, Mar. 2015.

[10] B. Lin, Y. Sun, J. E. Sanchez, and X. Qian, "Efficient vessel feature detection for endoscopic image analysis," *IEEE Trans. Biomed. Eng.*, vol. 62, no. 4, pp. 1141–1150, Apr. 2015.

[11] S. Wang *et al.*, "Computer-aided endoscopic diagnosis without human-specific labelin," *IEEE Trans. Biomed. Eng.*, vol. 63, no. 11, pp. 2347–2358, Nov. 2016.

[12] G. A. Puerto-Souza, J. A. Cadeddu, and G. L. Mariottini, "Toward long-term and accurate augmented-reality for monocular endoscopic videos," *IEEE Trans. Biomed. Eng.*, vol. 61, no. 10, pp. 2609–2620, Oct. 2014.

[13] T. Parpala-Spårman, I. Paananen, M. Santala, P. Ohtonen, and P. Hellström, "Increasing numbers of ureteric injuries after the introduction of laparoscopic surgery," *Scand. J. Urol. Nephrol.*, vol. 42, no. 5, pp. 422–427, 2008.

[14] W.-J. Fu, Z.-X. Wang, G. Li, F.-Z. Cui, Y. Zhang, and X. Zhang, "Comparison of a biodegradable ureteral stent versus the traditional double-J stent for the treatment of ureteral injury: An experimental study," *Biomed. Mater.*, vol. 7, no. 6, p. 065002, 2012.

[15] D. Chung, J. Briggs, B. W. Turney, and C. R. Tapping, "Management of iatrogenic ureteric injury with retrograde ureteric stenting: An analysis of factors affecting technical success and long-term outcome," *Acta Radiol.*, vol. 58, no. 2, pp. 170–175, 2016.

[16] Z. Wei, F. Guo, Y. Gao, Y. Zhao, C. P. Hospital, and Y. M. Hospital, "Application of ureteral catheter in the prevention of ureteral injury under gynecologic laparoscopic surgery," *China Health Standard Manage.*, vol. 33, no. 6, pp. 26–27, 2015.

[17] J. M. Teichman, J. E. Lackner, and J. M. Harrison, "Comparison of lighted ureteral catheter luminance for laparoscopy," *Tech. Urol.*, vol. 3, no. 4, pp. 213–215, 1997.

[18] T. Jing, C. Zhang, and L. Jiang, "A novel retrieval technique for ureteral stents under ultrasound guidance in male patients," *Urology*, vol. 106, pp. 226–230, Aug. 2017.

[19] E. Tanaka, S. Ohnishi, R. G. Laurence, H. S. Choi, V. Humblet, and J. V. Frangioni, "Real-time intraoperative ureteral guidance using invisible near-infrared fluorescence," *J. Urol.*, vol. 178, no. 5, pp. 2197–2202, 2007.

[20] S. Siddighi, J. J. Yune, and J. Hardesty, "Indocyanine green for intraoperative localization of ureter," *Amer. J. Obstetrics Gynecol.*, vol. 211, no. 4, pp. 436.e1–436.e2, 2014.

[21] F. P. R. Verbeek *et al.*, "Intraoperative near infrared fluorescence guided identification of the ureters using low dose methylene blue: A first in human experience," *J. Urol.*, vol. 190, no. 2, pp. 574–579, 2013.

[22] M. Al-Taher, J. van den Bos, R. M. Schols, N. D. Bouvy, and L. P. S. Stassen, "Fluorescence ureteral visualization in human laparoscopic colorectal surgery using methylene blue," *J. Laparoendoscopic Adv. Surg. Techn.*, vol. 26, no. 11, pp. 870–875, 2016.

[23] E. Song *et al.*, "A novel endoscope system for position detection and depth estimation of the ureter," *J. Med. Syst.*, vol. 40, no. 12, p. 266, 2016.

[24] F. Yu, E. Song, H. Liu, Y. Li, J. Zhu, and C.-C. Hung, "An augmented reality endoscope system for ureter position detection," *J. Med. Syst.*, vol. 42, no. 8, p. 138, 2018.

[25] E. Song, F. Yu, Y. Li, H. Liu, Y. Wan, and C.-C. Hung, "An image-guided endoscope system for the ureter detectio," *Mobile Netw. Appl.*, vol. 23, no. 6, pp. 1655–1668, 2018.

[26] J. C. Castillo, A. Fernández-Caballero, J. Serrano-Cuerda, M. T. López, and A. Martínez-Rodrigo, "Smart environment architecture for robust people detection by infrared and visible video fusion," *J. Ambient Intell. Hum. Comput.*, vol. 8, no. 2, pp. 223–237, 2017.

[27] P. Zhu and Z. Huang, "A fusion method for infrared–visible image and infrared-polarization image based on multi-scale center-surround top-hat transform," *Opt. Rev.*, vol. 24, no. 3, pp. 370–382, 2017.

[28] P. Stajanca *et al.*, "Effects of gamma radiation on perfluorinated polymer optical fibers," *Opt. Mater.*, vol. 58, pp. 226–233, Aug. 2016.

[29] W. Zhang, A. Abang, D. J. Webb, and G. D. Peng, "Wavelength drift of PMMA-based optical fiber Bragg grating induced by optical absorption," *IEEE Photon. Technol. Lett.*, vol. 27, no. 4, pp. 336–339, Feb. 15, 2015.

[30] J. Huang, D. Kremenakova, J. Militky, and F. B. Mazari, "Strength distribution of PMMA plastic optical fiber," *Ind. Textile*, vol. 66, no. 5, pp. 265–268, 2014.

[31] A. R. Prado *et al.*, "Polymethyl methacrylate (PMMA) recycling for the production of optical fiber sensor systems," *Opt. Express*, vol. 25, no. 24, pp. 30051–30060, 2017.
[32] H. J. Kim, "Sendust-based poly-tetra-fluoro-ethylene composite electromagnetic absorber by aerosol deposition," *J. Nanoelectron. Optoelectron.*, vol. 10, no. 3, pp. 376–380, 2015.
[33] A. Jain and K. Vijayan, "Effect of thermal aging on the crystal structural characteristics of poly (tetra fluoro ethylene)," *Polym. Eng. Sci.*, vol. 47, no. 11, pp. 1724–1729, 2007.
[34] H. F. Ng, "Automatic thresholding for defect detection," *Pattern Recognit. Lett.*, vol. 27, no. 14, pp. 1644–1649, 2006.
[35] H. V. H. Ayala, F. M. dos Santos, V. C. Mariani, and L. dos Santos Coelho, "Image thresholding segmentation based on a novel beta differential evolution approach," *Expert Syst. Appl.*, vol. 42, no. 4, pp. 2136–2142, 2015.
[36] K. Tsakmakidis, "Scattered light for white leds," *Nature Mater.*, vol. 12, no. 6, p. 472, 2013.
[37] M. Chen, X. Shi, Y. Zhang, D. Wu, and M. Guizani, "Deep features learning for medical image analysis with convolutional autoencoder neural network," *IEEE Trans. Big Data*, to be published, doi: 10.1109/TBDATA.2017.2717439.
[38] M. Chen, Y. Zhang, M. Qiu, N. Guizani, and Y. Hao, "SPHA: Smart personal health advisor based on deep analytics," *IEEE Commun. Mag.*, vol. 56, no. 3, pp. 164–169, Mar. 2018.
[39] M. Chen, Y. Ma, Y. Li, D. Wu, Y. Zhang, and C.-H. Youn, "Wearable 2.0: Enabling human-cloud integration in next generation healthcare system," *IEEE Commun. Mag.*, vol. 55, no. 1, pp. 54–61, Jan. 2017.
[40] M. Chen, Y. Hao, K. Hwang, L. Wang, and L. Wang, "Disease prediction by machine learning over big data from healthcare communitie," *IEEE Access*, vol. 5, pp. 8869–8879, 2017.

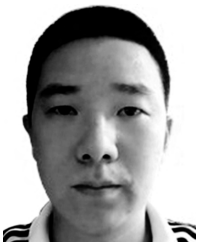

FENG YU received the M.S. degree from the School of Electronic and Electrical Engineering, Wuhan Textile University, in 2012. He is currently pursuing the Ph.D. degree with the School of Computer Science and Technology, Huazhong University of Science and Technology. His research interests include medical image processing, optical imaging research, medical device development, machine learning, and wireless localization technologies.

ENMIN SONG received the Ph.D. degree in electrical engineering and computer science from Teesside University, U.K. After completing the Ph.D. degree, he was a Postdoctoral Researcher with the University of California at San Francisco. He is currently a Professor with the School of Computer Science and Technology, Huazhong University of Science and Technology, China. His current research interests include medical image processing and medical image information analysis. He is a Senior Member of the IEEE.

HONG LIU received the Ph.D. degree in electrical engineering and computer science from Teesside University, U.K. She is currently a Professor with the School of Computer Science and Technology, Huazhong University of Science and Technology, China. Her current research interests include medical image processing, pattern recognition, and algorithmic design and analysis.

JUN ZHU received the bachelor's degree from the School of Computer Science and Technology, Huazhong University of Science and Technology, in 2016, where he is currently pursuing the master's degree. His research interests include image recognition technique and its application in endoscopic image.

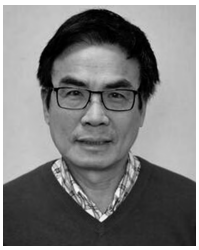

CHIH-CHENG HUNG was with Intergraph Corporation, from 1990 to 1993, for the research and development of remote sensing image processing software. He is associated with the Laboratory for Machine Vision and Security Research, Kennesaw State University, Kennesaw, GA, USA, where he is currently a Professor of computer science. His research interests include image processing, pattern recognition, and artificial intelligence.